electronics

MDPI

Article

Current Source Strategy for Energy Injection from a CapMix Cell

María G. Busto, Miguel J. Prieto, Juan A. Martín-Ramos, Juan A. Martínez and Alberto M. Pernía *

Department of Electrical Engineering, Universidad de Oviedo, Campus Universitario, EDO 3, 33203 Gijón, Spain; gonzalezbusmaria@uniovi.es (M.G.B.); mike@uniovi.es (M.J.P.); jamartin@uniovi.es (J.A.M.-R.); jamartinez@uniovi.es (J.A.M.)

* Correspondence: amartinp@uniovi.es; Tel.: +34-985182566

Abstract: Circulation of salty and fresh water through the electrodes of a deionization cell produces a voltage between the electrodes caused by the Capacitive Donnan Potential (CDP). The voltage so generated is very low (100 mV), but this work demonstrates that it is possible to develop a power converter suitable to inject this energy into the grid or into energy storage systems; this is a relevant aspect of this paper, for most works in the literature simply dissipate this energy over a resistor. To increase the input voltage, a stack of electrodes is connected in series. A bridgeless rectifier that uses a dual buck–boost converter to operate with both the positive and negative cycles is used to extract the energy from the cell. The topology chosen, which is operated as a current source, can work at extremely low voltage levels and provide power factor correction. After this stage, an H-bridge inverter can be included to inject the energy into the AC grid. The whole system implements a hysteresis control system using the current through the inductor of the power converter as control variable. This paper investigates the influence of such current on the efficiency of the total system.

Keywords: CapMix cell; Capacitive Donnan Potential (CDP); supercapacitor; low-voltage energy harvesting; up/down converter; power factor correction (PFC); salinity gradient; hysteresis control

Citation: Busto, M.G.; Prieto, M.J.; Martín-Ramos, J.A.; Martínez, J.A.; Pernía, A.M. Current Source Strategy for Energy Injection from a CapMix Cell. *Electronics* **2024**, *13*, 42. https://doi.org/10.3390/electronics13010042

Academic Editors: Mohamed Benbouzid, Sinisa Durovic, Xiandong Ma and Hao Chen

Received: 28 November 2023
Revised: 15 December 2023
Accepted: 17 December 2023
Published: 20 December 2023

1. Introduction

More than 73.5% of the electricity used around the globe is obtained from fossil fuels such as coal, natural gas or crude oil [1]. The massive use of this type of resources has led to large concentrations of greenhouse gases (GHG) in the atmosphere. This is especially true when considering carbon dioxide emissions coming from the combustion of the above-mentioned fossil fuels. In particular, electricity and heat generation caused the biggest increase in CO_2 emissions in 2021, at 46% of the global increase [2].

Globally, there is an increasing awareness of the need to limit GHG pollution into the atmosphere, and this is why energy production is slowly turning towards environment-friendly solutions based on the use of renewable energy sources. Solar power, wind power, hydroelectric power, biomass and ocean energy are the best-known sources of this kind. But there is another form of green energy that can also contribute to the low-emission goal: so-called blue energy [3].

Blue energy, also known as salinity-difference energy, exploits the free energy released when two solutions with different salinity concentrations combine, as constantly occurs at river bodies [4]. This must be definitely considered as a renewable form of energy, since it is the sun-powered global hydrological cycle that continuously makes water evaporate from the sea and precipitate as fresh water into river runoff. Additionally, salinity gradient energy may also be extracted from natural or industrial brine discharge, which can provide larger salinity gradients and thus higher energy. In any case, engineered solutions must be used to avoid fouling [5].

Over the past few decades, remarkable advances in fundamental studies, experimental investigations and field investigations have been carried out towards finding out how to harvest this salinity gradient energy in an efficient way. This has given rise to thorough

analyses seeking to determine the appropriate design and disposition of salinity gradient energy conversion devices to maximize the energy obtained or to avoid fouling [6,7]. However, no indication of how to then extract that energy is usually given. Also, most of the solutions proposed are associated with membrane-based techniques: Pressure Retarded Osmosis (PRO) and Reverse Electrodialysis (RED) [8].

PRO generates electricity by using a hydro-turbine that is fed with the pressurized water obtained thanks to the osmotic pressure difference created between two chambers. RED, on the other hand, makes diluted and concentrated solutions flow into a cell, where ionic exchange membranes succeed in creating an electrical potential across the electrodes of the cell, and some redox reaction appears [8,9].

Unfortunately, these methods are still used on a laboratory scale only. There have been major advances, but commercial products are still far from being available. The main drawbacks that remain to be solved are related to the efficiency and price of the membranes, together with gas generation in the case of RED [10], and the need to use dynamos or turbines in PRO [11].

Due to the setbacks of the techniques mentioned above for blue energy harvesting, another alternative has been proposed: CapMix (Capacitive Mixing). This technique uses ultra-capacitor materials to produce devices that can benefit from the salinity gradient created using sea and river water to perform as an electricity source. By storing the energy harvested in something that performs like an ultra-capacitor, the transfer of this energy to the grid or to other electrical energy storage systems will be simplified. CapMix is the technique that will be studied in this paper as part of a renewable energy system to inject power into a battery or into the grid.

CapMix methods allow one to directly extract electrical energy without the need to use electromechanical converters, such as turbines or heat engines, or redox reactions. CapMix is based on the variation in the potential difference between two nanoporous electrodes caused by exchanging the ionic contents of the solution in contact with them. Three CapMix techniques can be differentiated: Capacitive Double Layer Expansion (CDLE), Capacitive Donnan Potential (CDP) and Mixing Entropy Battery (MEB), which merges both CDLE and CDP. CDLE requires an external power supply to charge the electrodes; CDP uses perm-selective membranes so that only one type of ion flows through them [12,13]; MEB uses reactive electrodes to extract the blue energy stored in the form of chemical energy.

An analysis of the energy production through CapMix techniques [14] reveals different values depending on the actual technique used and on the salinity concentration [15]. Thus, CDLE can generate 0.05 W/m^2, whereas the incorporation of membranes increases the energy production to values of 0.2 W/m^2 in the case of CDP or 0.4 W/m^2 for mixing entropy batteries (MEBs), at the cost of increasing the complexity of the electrodes [16,17]. The present work focuses on CDP, since its average power density is four times higher than that of CDLE. It is still lower than that of MEBs, which currently produce the highest power, but this technology is not considered in this paper because of the potential risk of polluting the environment due to the copper included in the electrodes used. It must be noted, in any case, that all these techniques are limited by: (a) self-discharge processes; (b) the duration of the salt and fresh water exchange cycles; and (c) the high internal resistance, especially when the cell incorporates fresh water. The last two parameters are especially important, and reducing them will greatly influence the energy production capacity of the cell [16]. On the one hand, the higher the internal resistor, the higher the losses when extracting the energy harvested by the CapMix cell; optimization of this parameter is fully dependent of the materials and structures used to manufacture such a cell. On the other hand, the shorter the time needed to extract the energy from the cell, the higher the number of charge/discharge cycles per unit of time and, hence, the higher the daily amount of energy that can be extracted; this time depends both on the internal parameters of the cell itself and on the discharge process defined to extract the harvested energy.

Figure 1 sketches the working principle of a CapMix Cell based on the Donnan Potential (CDP). When salt water enters the cell, ions diffuse through the exchange membranes

and are embedded onto the capacitive electrodes (violet arrows represent movement of anions; yellow arrows represent movement of cations). This originates an electronic current in the external circuit (red arrow) flowing from the anion-adsorbing electrode to the cation-adsorbing electrode through an external load to compensate the ionic charge that forms within the porous electrodes (Figure 1a). If, right after this, fresh water passes through the cell, the ions that had been deposited on the electrodes flow through the exchange membranes into the flowing solution. This causes the electrodes to be discharged, and electrons flow back from the cation-adsorbing electrode to the anion-adsorbing electrode through an external load, which again constitutes current flow (Figure 1b). Therefore, by alternating the flow of freshwater and saltwater into the cell, an AC voltage can be obtained across the cell electrodes that gives rise to continuous power production. It must be noted that no electrochemical reaction is required (electron and ion flow is purely of a capacitive nature) and, therefore, there is no need for a chemical redox reaction in the system [18].

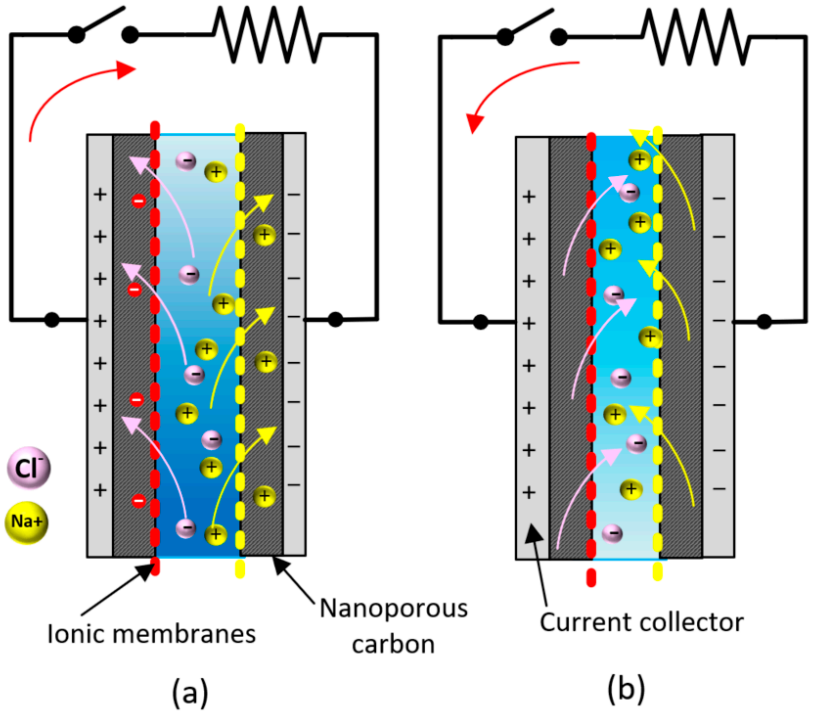

Figure 1. (**a**) Charging process of the CapMix cell with a concentrated solution. (**b**) Discharge process of the CapMix Cell with a diluted solution [1].

CapMix cells share certain properties with supercapacitors, and they even use similar electrical models in their characterization. The fundamental characteristic that they share is that the operation of both types of devices is based on retaining ions without generating redox reactions. Even so, there are substantial differences in their behavior. Supercapacitors retain ions from an electrolyte through the external application of an electric field [19], whereas ion movement in CapMix cells occurs by diffusion through ionic membranes where the electrolyte changes from salt water to fresh water. This fundamental difference causes lower voltage increases in the CapMix cell and variations in the series resistance with the salt concentration of the circulating water [15]. Supercapacitors have a series resistance of typically a few tens of mΩ, with power densities greater than 400 mW/g (for an effective area of 1000 m^2/g) and efficiencies of 95% in the charge–discharge processes. CapMix cells, however, present a series resistance that changes from hundreds of mΩ with salt water to several ohms with fresh water; this reduces the efficiency and limits the energy production to 2.7 mW/g.

Research on capacitive energy extraction from salinity gradients has given rise to important contributions related to materials performance, cell architecture or operating parameters of the solution flowing through the cell (temperature, velocity, etc.) [15]. How-

ever, CapMix experiments usually connect the cell to a resistive load that instantaneously utilizes the stored energy. The value of this resistive load determines the energy transfer and is sometimes considered as an additional parameter to take into account [20]. This is obviously not what must be expected from an energy supply device. Zou et al. [15] studied the behavior of CapMix cells under different operating modes, but the extraction of energy from the cell was always done by direct connection to an external resistance. The value selected for this resistance affects the current and voltage in the cell, thus conditioning the energy generated. This situation changes when the circulating current is constant during the discharge process, as will be introduced later. So far, the power electronics system required to adequately extract the energy from the CapMix cell has not been deeply analyzed yet, and this is one of the contributions of the present paper.

Currently, there are two major complications for blue energy harnessing. On the one hand, it may not be easy to find adequate areas to place salinity-differential energy systems. On the other hand, it is not clear how to efficiently convert blue energy into really usable energy. The latter challenge is the backbone of this paper, which partly deals with harvesting the energy from the capacitive cells and feeding it into the AC mains, or into a battery. Several applications can be found in the literature where energy is stored in batteries and/or supercapacitors, but these applications are mostly focused on mobility and microgrids, with a primary source completely different from the one considered in this paper. Therefore, the electronic converters around these applications cannot be directly used to extract energy from a CapMix cell. This requires a front-end high gain step up converter; one possibility is presented in this work.

2. Characteristics of the CapMix Cell

The main goal of CapMix cells is adsorbing as many ions as possible once they have flowed through the corresponding ion exchange membranes: the larger the amount of ions on the electrodes, the higher the energy stored. This is why these electrodes are designed to have the largest possible surface—and hence give rise to the largest possible cell capacitance. In order to further increase this surface, the current collectors of CapMix cells (typically made of graphite or titanium) are covered with activated carbon deposits, which have a high specific surface area [21–23].

As already stated, CapMix cells share certain properties with supercapacitors, which enables them to use the same models as the latter. The operational principle of a supercapacitive system is based on its electrical double layer (EDL) structure. Recently, there has been an increase in the use of supercapacitors in the field of power electronics. To facilitate the accurate design and simulation of these systems, there is a need to make use of accurate and well-validated models [13].

Throughout the years, several electrical models have been proposed to predict the electrical behavior of an EDLC (Electrical Double Layer Capacitor), the simplest of which is the classical equivalent circuit model shown in Figure 2a. This model has only three parameters: a capacitor (C), an equivalent series resistance (R_S) representing ohmic losses in the EDLC, and a parallel resistance (R_P) representing losses due to leakage current in the EDLC. The ease with which the parameters of this model are determined makes this the most commonly used model, and it is used in this work to reduce the computing time of the simulations carried out.

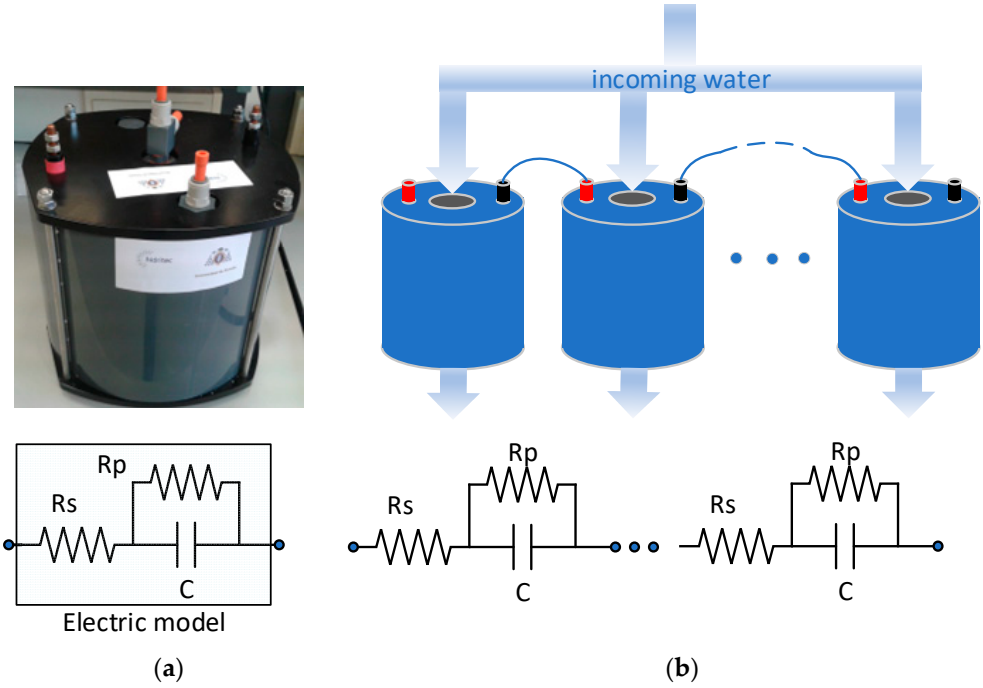

Figure 2. (**a**) CapMix model. (**b**) Series cascaded CapMix cells.

The analysis of the diffusion of the ions and the formation of the double layer would require the complex modeling at the electrochemical level to understand the correct internal operation of the cell [15,23]. However, for the design of the power stages in charge of managing the energy stored, simple electrical models are used that fundamentally allow for quantifying the energy and the power dissipation. In this regard, it is common to model this type of cell by means of the simple supercapacitor model indicated above ($C + R_S + R_P$). Despite the simplicity of this model, it proves very useful in the subsequent design of electronic converters [24,25].

The voltage across CapMix cells can also be increased by stacking them in series/parallel (to increase the voltage while keeping the series resistance low). This is also a common strategy when using other primary sources such as fuel cells, for instance [26], but CapMix cells perform differently. The voltage provided by a CapMix cell (0.1 V) is 10 times lower than that obtained from a single fuel cell (1 V). Therefore, to obtain similar voltages, around ten CapMix cells would have to be connected in series for each single fuel cell. This brings about a problem related to variations in the capacitance of different CapMix cells due to manufacturing tolerances, which would cause significant voltage variations for the same discharge current that would make it necessary to incorporate equalization circuits, thus increasing the complexity of the system and reducing its efficiency.

This paper provides a full electrical characterization of an individual cell, which later allows the models thus obtained to be interconnected in the same way as the cells are [27]. Figure 2b shows some of these stacks, which end up performing like a supercapacitor. The separation between the activated carbon electrodes inside the cell can also be optimized to obtain an equivalent capacitor that provides the maximum possible energy density.

The parameters of the CapMix cell based on the classical equivalent circuit model can be determined by using a cell initially cleaned with distilled water to eliminate possible ions on the electrodes [28,29]. Then, saline water of a particular concentration flows into the cell, after which the terminals are connected to a DC current source that charges the cell by causing the ions to be continuously deposited on the electrodes. The result is equivalent to charging capacitance C, which will go through a self-discharge process when the current source is disconnected from the cell. This process is depicted in Figure 3.

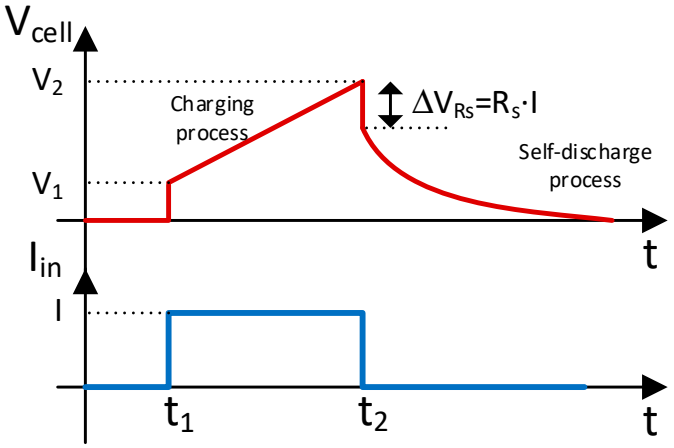

Figure 3. Variation of voltage across the CapMix cell during its charge and discharge.

From the waveforms shown in Figure 3, it can be seen that R_S is determined from the step undertaken by the cell voltage when the charge or the discharge starts. Hence, by mere application of Ohm's law, we derive:

$$R_S = \frac{\Delta V_{Rs}}{I} \tag{1}$$

If the charging process is considered to be linear (as is the case when a DC current flows through a capacitor), the value of capacitance C can be derived from Equation (2).

$$V_2 - V_1 \approx \frac{I}{C}(t_2 - t_1) \tag{2}$$

Finally, the evolution of the cell voltage during the self-discharge of the cell is determined by Equation (3) where $V_{C_{max}}$ is the initial voltage of the discharge.

$$V_{Cell} \approx V_{C_{max}} \cdot e^{-t/(R_P \cdot C)} \tag{3}$$

which can be used to derive the leakage resistance by selecting any two points ((t_{p1}, V_{p1}) and (t_{p2}, V_{p2})):

$$R_P = -\frac{t_{p1} - t_{p2}}{C \cdot \ln\left(\frac{V_{p1}}{V_{p2}}\right)} \tag{4}$$

The energy that can be extracted from a CapMix cell depends on the values calculated with Equations (1)–(4). Since this energy is also dependent on the concentration of the solution between the electrodes (M), the surface of the electrodes in contact with the solution (S), the distance between the electrodes (d) and the number of electrodes connected in series (n) and in parallel (m), it is obvious that all these parameters indirectly influence the values of the series resistance, the parallel resistance and the capacitance of the cell.

To better understand the behavior of this type of cell, a commercial cell (Voltea C-3, Figure 2) has been tested by performing the test depicted in Figure 3 and characterized using expressions (1) to (4) on the plot thus obtained, which can be seen in Figure 4. This resulted in C = 16,000 F ($\Delta t \approx 430$ s, $\Delta V \approx 0.8$ mV), $R_P = 1\ \Omega$ and $R_S = 4\ m\Omega$ (for a 0.6 M salt concentration). Although there is an inherent nonlinearity that can be observed in Figure 4, a linear behavior in the cell is assumed (orange line), so that Equation (2) can still be used to estimate the capacity of the cell and, hence, the energy produced in each cycle. The manufacturer of C-3 cells specifies a nominal current of 120 A, which is a high value compared with the current used in the prototype. The cell has a very good stability after the first cycle, guaranteeing its correct charge saturation.

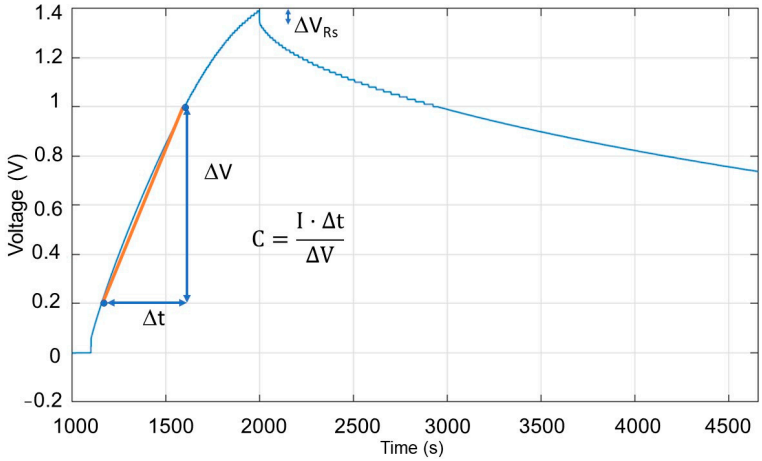

Figure 4. Voltage evolution during cell characterization (0.6 M, I = 30 A).

The commercial cell considered includes anionic and cationic membranes for the desalination of water using the capacitive deionization technique. This technique is actually based on the reverse of the process used by CapMix cells (salt ions present in the water are retained by application of an external voltage). Therefore, it can also be used to generate energy, since its internal configuration is exactly the same as that shown in Figure 1.

When water with different salt concentrations flows into the C-3 cell, a voltage of around 200 mVpp is obtained within a complete cycle: fresh water flowing into the cell during the first 5000 s followed by a flow of salt water (Figure 5). The voltage, and thus the total energy of the system, can be increased by connecting more cells in series; unfortunately, this will also result in a higher series resistance, thus limiting the maximum current that can be injected into the storage element (battery, supercapacitor, grid, etc.).

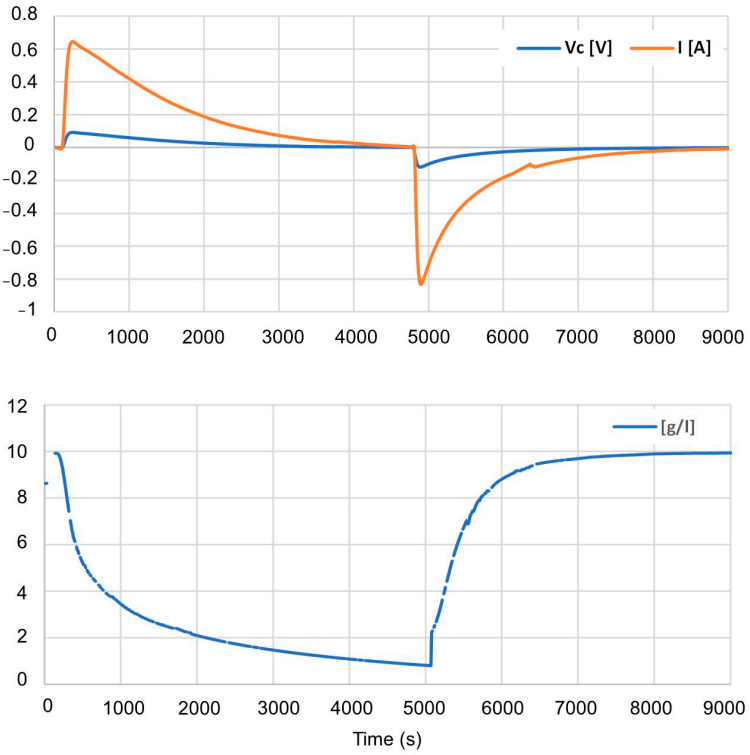

Figure 5. Top: Voltage (red curve) and current (blue curve) evolution obtained with a 0.123-Ω load. **Bottom**: Salt concentration evolution in a complete cycle.

3. Test Bench

The energy transfer from the CapMix cell into other systems, such as a battery or the grid, is one of the weakest points of the whole system. The power production of CapMix cells in the literature is tested by using an external resistor [15,22], but it is still necessary to describe how to effectively extract the energy stored in these cells.

In order to demonstrate the feasibility of developing a system suitable to harvest the energy generated thanks to the salinity gradient, a test bench has been implemented that allows this energy to be injected into an energy storage system (battery, supercapacitor) or into the AC grid. The main block in this test bench is an electronic converter that discharges the CapMix cell by forcing a certain current to flow out of it and then, by implementing a current-source behavior, injects the energy thus obtained into the selected storage system (a battery, the AC grid, etc.).

3.1. Electronic Converter Topology

Power topologies can be found in similar applications such as capacitive deionization (CDI) [24,25], where energy is transferred between CDI cells, making their voltage vary up to 2 V. Less related applications use supercapacitors or batteries as intermediate energy storage elements [30,31]. However, none of these applications involve voltage levels comparable to those present in CapMix cells. As already indicated at the end of Section 1, the literature is mainly focused on the charging process related to mobility applications [32,33] when the storage system is based on both supercapacitor and battery systems, but nothing has been found related to CapMix cells, which typically are loaded with a resistor [34], as primary sources with polarity inversion and very low voltage for energy transfer to the grid.

Due to the characteristics of CapMix cells (low output voltage of around 1 V and voltage inversion), a converter with a very high conversion ratio is required to inject the energy into the AC grid (230 V). In the test bench used, a buck–boost converter operating at the boundary between continuous and discontinuous conduction modes has been implemented. Although this type of converter cannot provide a high step-up voltage ratio by itself, it can be operated to perform as a current source and work with large voltage differences between input and output voltages, while injecting energy at the output, which is what is needed for the application described in this work. This topology has an additional advantage: the energy can also be transferred to any other energy storage systems, such as supercapacitors, regardless of whether the voltage of the storage system is higher or lower than that across the CapMix cell. In any case, it must be taken into account that the goal of the test bench implemented is demonstrating that energy can be efficiently extracted from these cells. Other alternatives for this topology must still be explored in future works.

Figure 6 shows a bridgeless dual buck–boost converter [35,36], which is suited to cope with both the positive and negative input voltages of the cell, and can provide a very high conversion ratio. The diodes used for the discharge of the inductors could be replaced with MOSFETS employing Zero Voltage Switching (ZVS) and Zero Current Switching (ZCS) in a synchronous rectification process to further improve the efficiency of the system [37]. As indicated, this bridgeless dual buck–boost converter is designed to operate in the so-called Boundary Conduction Mode (BCM), since this provides inherent power factor correction on the grid side.

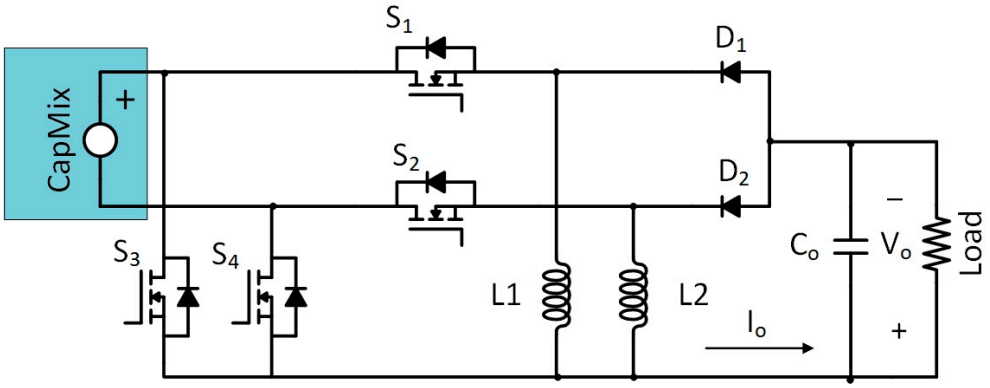

Figure 6. Bridgeless dual buck–boost converter.

3.2. Operating Principle

This topology is analyzed under the following assumptions:

- The converter operates in the BCM;
- Switch S4 is ON during the whole positive half-cycle of the Capmix cell, while S3 is ON during the negative one.

The performance of the converter considered is thoroughly analyzed in [36], and can be summarized in four stages.

Stage I: Switches S1 and S4 are on. Inductor L1 is energized by the input source. Current i_{L1} increases linearly from zero (S1 is turned on with zero current switching, ZCS; S4 is permanently on during the whole positive half-cycle, as already indicated). Diodes D1 and D2 are reverse biased.

Stage II: Switch S1 is turned off. Current i_{L1} freewheels via D1 (the energy stored in L1 is transferred to the load). The inductor is linearly discharged until current i_{L1} becomes zero.

Stages III and IV: Equivalent to Stages I and II when the input voltage is negative. Consider switches S2 and S3, inductor L2 and diode D2 instead.

3.3. Control Strategy

The adequate performance of the converter in our test bench is achieved by controlling the maximum and minimum values of the inductor current through a hysteresis current mode control, which needs no external oscillator or saw-tooth generator and responds quickly to transients [36].

This control strategy gives rise to variable frequency [38], since the input and output voltages are continuously changing and the switches are turned on and off, respectively, when the inductor current (I_{L_actual}) goes below a lower reference (I_{Lmin}) or above an upper limit (I_{Lmax}). This variable frequency does not necessarily involve higher EMI levels (international standard CISPR 11) if the switching is appropriately carried out (which can be achieved by employing ZVS and ZCS techniques, as suggested in Sections 3.1 and 3.2). Variable switching frequency might become an issue, however, when filtering the current to be injected into the storage element, since the corresponding filter will have to be calculated for the lower frequency present in the waveform. Section 3.4 discusses some alternatives to smooth the injected current.

The pair of switches to control is determined by implementing a polarity detector that detects the sign of the input voltage (see Figure 7). The efficiency of the whole converter will be determined by the peak values of the current established by the controller. Note that although the testbench presented in this paper operates in the BCM (hence, $I_{Lmin} = 0$), the controller described can be used to determine the maximum and minimum values of inductor current that maximize the efficiency of the energy harvesting system.

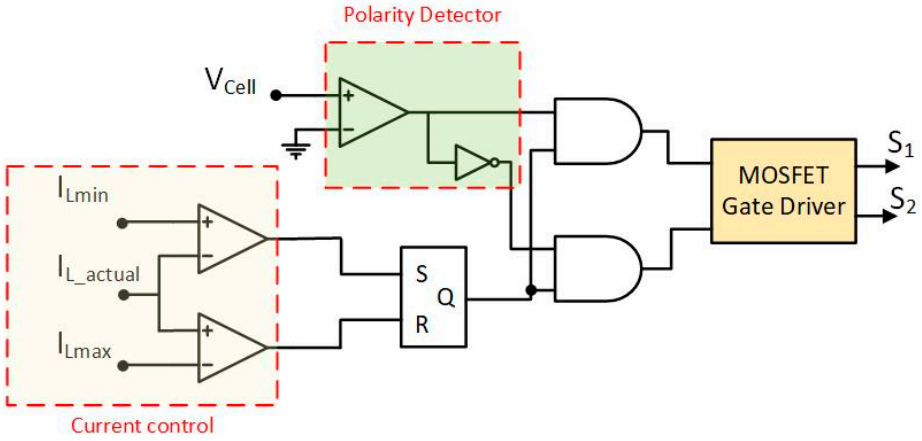

Figure 7. Block diagram of hysteresis current control.

3.4. Energy Transferring Process

The energy generated by the cell can be transferred either to a battery or directly to the AC grid using the topology described above. In the specific case of the test bench implemented, this energy can also be transferred to a supercapacitor thanks to the up/down capability of the converter chosen, which allows the charging process to proceed even if the supercapacitor is completely discharged.

If the load in Figure 6 is replaced by a battery, the proposed control system adjusts the switching-on time until the desired maximum current value is reached, and then switches off until the inductor current reaches the zero crossing (in the testbench considered, where $I_{Lmin} = 0$). The actual switching frequency varies as a function of the instantaneous values of the input and output voltages, and also as a function of the maximum inductor current.

The battery charging current comes directly from the discharge of the inductor converter. In this sense, the converter can be considered to have a current-source behavior [38,39], which allows for direct parallelization (Figure 8). Such parallelization of the converters enables the modularity of the system and reduces the injection of harmonics if the modules are conveniently interleaved (see Figure 9), without penalizing the performance of the overall system.

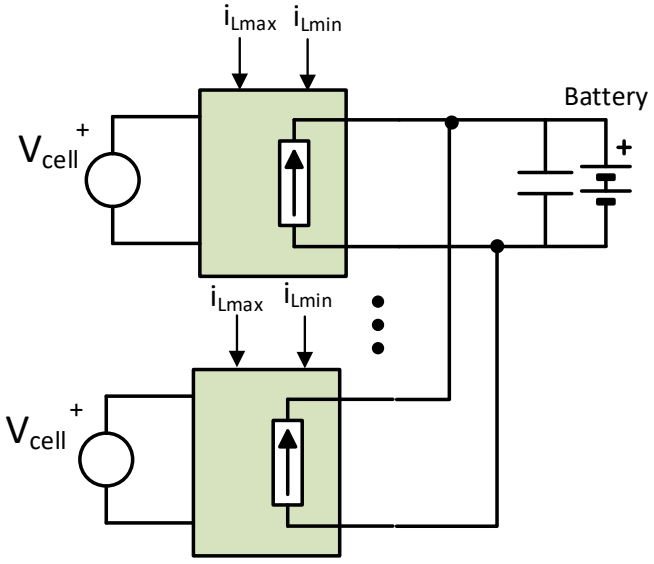

Figure 8. Converters' parallelization.

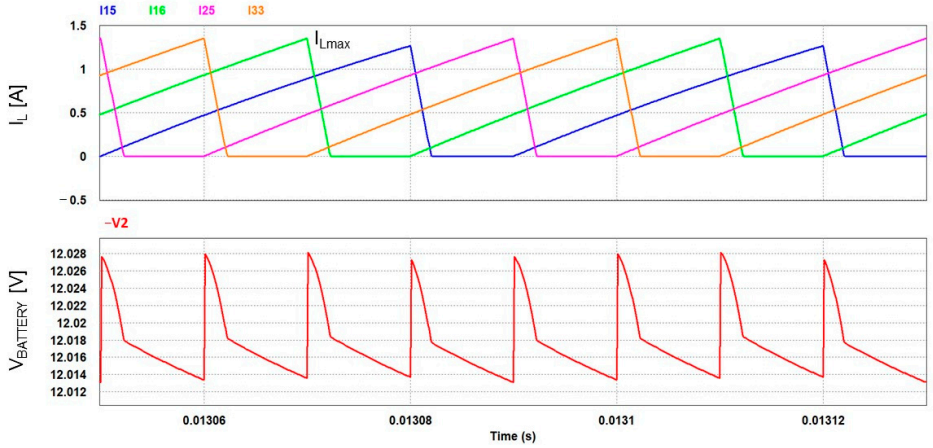

Figure 9. Inductor current and output voltage ripple simulation in a multiphase system (4-phase). $V_{BATTERY}$ = 12 V.

In Figure 9, we can see the result output by four converters in parallel operation, injecting current with shifted phase to increase the total current injected into the battery [40–43]. This will also reduce the high peaks in the current flowing into the battery, thus contributing to the lower degradation of the battery lifespan. By additionally incorporating a capacitive filter (200 µF), the current handled by the battery is significantly smoothed.

It might be discussed that operating the converter in the Continuous Conduction Mode (CCM) would reduce the current ripple and, hence, improve the quality of the current flowing into the battery. However, it has been found that this would give rise to a significant increase in the switching losses (which tend to be higher than conduction losses), resulting in a reduction in the converter efficiency. This is why operating the converter in BCM seems to be an interesting option for this application, since it allows for very simple control with the lowest possible switching losses.

If instead of using a battery we aim to transfer the energy from the bridgeless dual buck–boost converter into the AC grid, we need to connect a grid-synchronized inverter in between [39,40].

The bridgeless buck–boost converter must be controlled to perform as a current source injecting sinusoidal current into the grid through a bridge inverter operating in synchronism with the AC mains switching at 50 Hz (Figure 10). Such synchronization requires that zero crossings of the grid voltage be monitored.

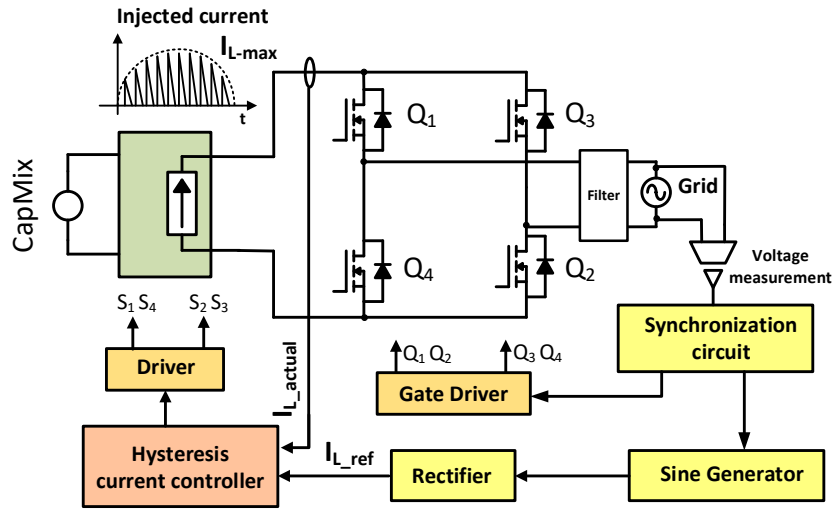

Figure 10. Block diagram of the control system to inject energy from the CapMix cell into the grid.

It can also be seen in Figure 10 that the reference for the inductor current is obtained from a rectifier whose input is a reconstruction of the grid voltage. This forces the current provided by the converter to have a sinusoidal shape, which is required to control the power transfer to the grid and the power factor [44].

Similarly to what was done in the case of the battery, it is possible to incorporate several converters in parallel to facilitate a reduction in the harmonics injected into the grid, as can be seen in Figures 11–13.

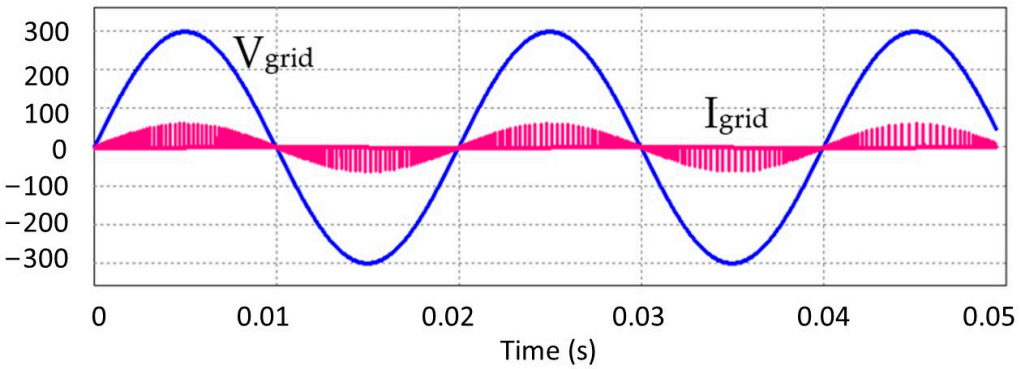

Figure 11. Simulated voltage and current through the AC grid without any filter.

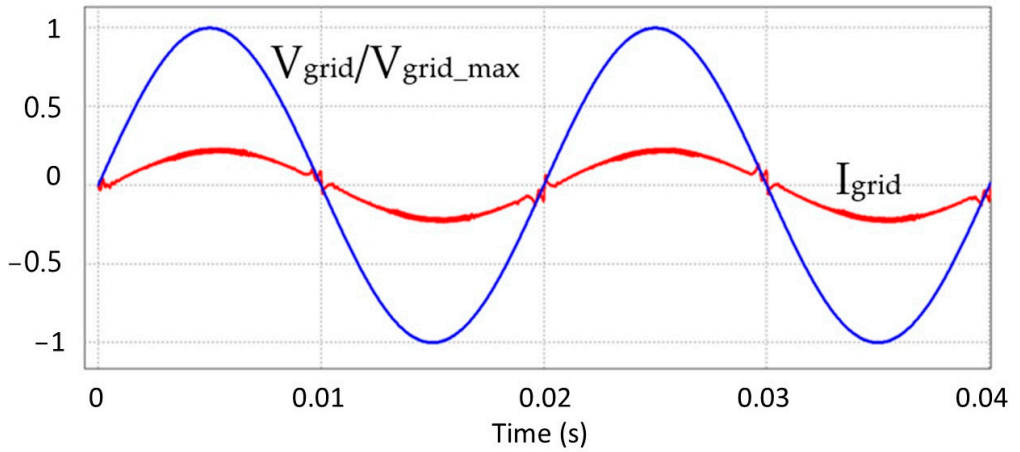

Figure 12. Simulated voltage and current through the AC grid with 4 interleaved converters in parallel and a CLC output filter (100 nF–20 mH–100 nF).

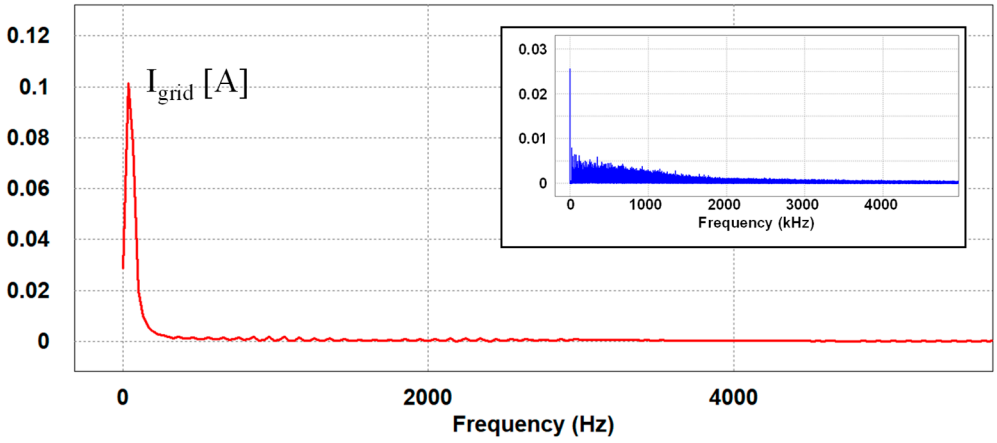

Figure 13. Simulated FFT of current through the AC grid with 4 interleaved converters in parallel and a CLC filter. Window: one converter with no filter.

4. Energy Production

This section presents an analysis that aims to evaluate the energy production capability of this technology. In order to do so, the Voltea C-3 desalination cell will be used as the CapMix cell under test, and it will be represented by the parameters measured in Section 2: C_1 = 16,000 F, R_{P1} = 1 Ω and R_{S1} = 4 mΩ. Since this cell can supply 100 mV when salt water flows in, 10 units are considered to be connected in series so as to increase the voltage up to 1 V. This connection results in an equivalent circuit with C = 1600 F, R_P = 10 Ω and R_S = 40 mΩ for the salt water cycle and C = 1350 F, R_P = 53 Ω and R_S = 120 mΩ for the fresh water cycle. Note the increase in the series resistance, which significantly affects the efficiency of the power transfer from the cell to the grid.

Figure 14 illustrates the process used to discharge the CapMix cell using a discharge current, I_d, that holds a constant value during a whole half-cycle. The cell starts charged with an initial voltage, V_{max}, and is linearly discharged with current I_d. The bottom plot of Figure 14 represents the evolution of the instantaneous power thus delivered by the cell. After a certain time, t_d, which depends on the cycle (fresh or salt water cycle), the cell will be fully discharged (V = 0 V; P = 0 W). Note that the minimum time required for discharging the cell (t_d) is a characteristic parameter of the cell itself and does not depend on the number of cells connected in series or parallel.

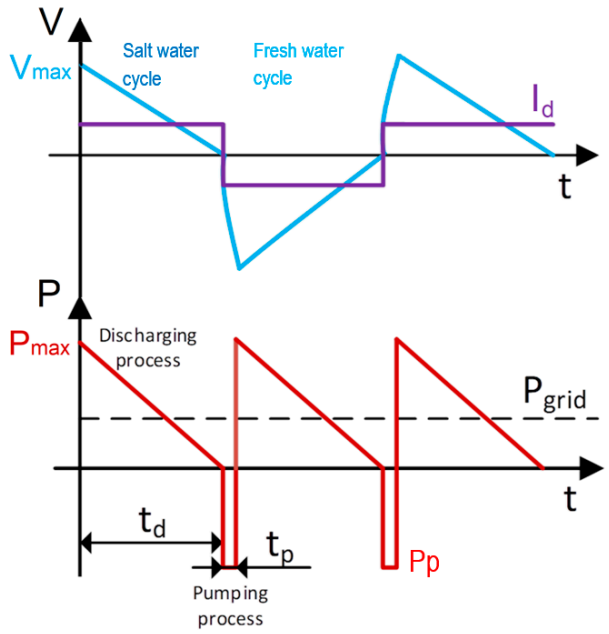

Figure 14. Energy injection from the CapMix cell into the grid, assuming a constant discharge current, I_d.

Once the cell has been discharged, it must be charged again by making water with a different salinity flow in. The pumping time, t_p, required to replace the water inside the cell also involves some power consumption, P_p, which is another parameter to determine the total energy produced. According to the power evolution represented in Figure 14, the average power transferred to the AC grid is:

$$P_{grid} = \frac{\frac{1}{2}\cdot P_{max}\cdot t_d - P_p\cdot t_p}{t_d + t_p} \quad (5)$$

Using the plot in Figure 14, it is simple to calculate the energy that can be extracted from the cell every cycle. Knowing that these cycles are repeated every t_d + t_p seconds, the ideal daily energy (E) that can be obtained is given by:

$$[kJ/day] = \frac{1}{2}\cdot C\cdot\left(V_{max}^2 - V_f^2\right)\cdot\frac{24\cdot 3.6}{t_d + t_p} \quad (6)$$

In this expression V_f is the final voltage across the equivalent capacitor of the cell. It might seem sensible to make this value be 0 V (so that there is no energy left to extract in the capacitor), but this parameter will be further analyzed in a later section.

Equation (6) also neglects the energy demanded by the pump. The energy consumption of the pumping system is estimated to be 5% of the total energy produced [16]. Therefore, in order to reduce the influence of t_p, it is also important to reduce the processed water volume by reducing the distance between the electrodes in the cell. Note that increasing the number of CapMix cells in series or parallel involves larger water volume, but the pressure drop in the hydraulic system does not increase significantly because all the cells are fed in parallel (see Figure 2).

Each Voltea C-3 cell uses around 3 L, which, in the example considered, involves pumping 30 L. With a typical commercial water pump of 2400 L/h, 30 L can be injected into the 10 cells in t_p = 45 s.

As far as the discharge time, t_d, is concerned, it will be obtained by ensuring that the capacitor is discharged at the current that provides the maximum possible power transfer, where R_L is the inductor resistance and R_{ON} is the switch resistance ($R_T = R_S + R_{ON} + R_L$).

$$I_d = \frac{V_C}{2 \cdot (R_s + R_{ON} + R_L)} \tag{7}$$

It must be noted, however, that the actual discharge current is that flowing through the inductor of the power converter used to extract the energy out of the CapMix cell. In the case of the testbench used, and assuming an equivalent circuit to that in Figure 2 connected to the input of the dual bridgeless buck–boost converter, the maximum inductor current that can be reached during Stage I (when the energy of the cell is transferred to the inductor) depends on the series resistances of the cell (R_S), which also depend on the salt or fresh water cycle, the inductor (R_L) and the switch (R_{ON}) used.

Once the current through the inductor reaches the value I_{Lmax}, the converter must change to Stage II (inductor discharge on the output), otherwise the current will remain constant, the energy stored in the inductor will not increase, and more losses will be added to the system. Considering the buck–boost converter operating in the BCM, as indicated in Section 3.1, the value of I_{Lmax} is:

$$I_{Lmax} = 2 \cdot I_d \tag{8}$$

Assuming the electrical model of the cell (Figure 2a), the evolution of the capacitor voltage (V_C) that starts with an initial voltage $V_c(0)$ is not completely linear due to the parasitic parallel resistance:

$$V_C(t) = V_C(0) \cdot e^{-t/R_p C} - I_d \cdot R_p \left(1 - e^{-t/R_p C}\right) \tag{9}$$

If a discharge current I_d is selected at each moment of the discharge process using Equation (7), an expression for the discharge time, t_d, can finally be derived for each salt or fresh water cycle, as indicated in (10):

$$t_d = -R_p C \cdot \ln \left[\frac{V_f \cdot \left(1 + \frac{R_p}{2R_T}\right)}{V_C(0) + V_f \cdot \left(\frac{R_p}{2R_T}\right)} \right] \tag{10}$$

To estimate the energy obtained, resistive losses E_d in the series resistance of the cell, which depends on the cycle considered, are discounted.

$$E_d = \int_0^{t_d} R_s \cdot I_d^2(t)\, dt = \int_0^{t_d} R_s \cdot \frac{V_C^2(t)}{4R_T^2}\, dt \tag{11}$$

Parallel losses in the R_p resistance are almost negligible due to the low cell voltage (V_{Cell}) and high R_p. Then the total energy produced in one cycle (salt or fresh water) is:

$$E[^{kJ}/_{cycle}] = \left[\frac{1}{2}\cdot C\cdot\left(V_{max}^2 - V_f^2\right) - E_d\right] \quad (12)$$

The average daily energy production in our system depends on how many cycles like the one represented in Figure 14 can take place in 24 h. Therefore, it might be preferable to leave some energy unextracted if this means that more cycles can be produced throughout the day. The presence of V_f in Equation (12) represents this situation: having a final cell voltage different from 0 affects the total discharge time and, hence, the number of charge/discharge cycles per day and the daily energy production (Figure 15).

$$E[^{kJ}/_{day}] = [(E_{salt} + E_{fresh})]\cdot\frac{24\cdot 3.6}{t_{d\_salt} + t_{d\_fresh} + 2t_p} \quad (13)$$

where E_{salt} and E_{fresh} are the energy produced during the salt and fresh water cycles, respectively. In a similar way, t_{d_salt} and t_{d_fresh} represent the discharge times for each cycle.

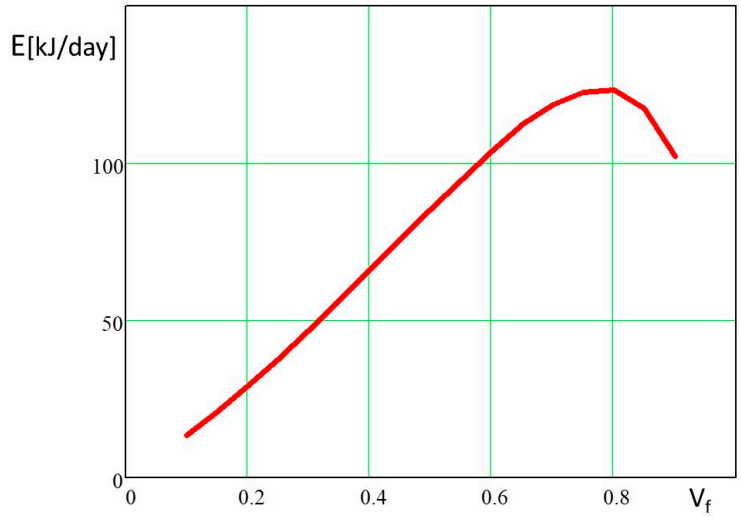

Figure 15. Daily energy production from the CapMix cell as a function of V_f [V].

In all the analyses carried out so far, the discharge current, I_d, obtained from Equation (7) is continuously changing as a function of the instantaneous value of the voltage in the equivalent capacitor. This value provides the maximum power transfer (at the discharge cycle level), but might complicate the control of the DC/DC converter. Another strategy would be to fix the I_d current during the entire discharge process. In this case, the discharge time only depends on the selected current:

$$t_d = \frac{C\cdot(Vc(0) - V_f)}{I_d} \quad (14)$$

And the energy losses in cell can be obtained from:

$$E_d = R_S\cdot I_d^2\cdot t_d = R_S\cdot I_d\cdot(V_C(0) - V_f)\cdot C \quad (15)$$

Using these expressions in Equation (13), it is possible to derive the daily energy production as a function of the discharge current chosen (Figure 16), where the final discharge voltage plays an important role. There are two opposing effects: on the one hand, increasing the current allows more cell discharge cycles per day and therefore higher energy production, and on the other hand, increasing the current leads to higher conduction

losses. The combination of both effects leads to an evolution as shown in Figure 16, and to a maximum for a given discharge current.

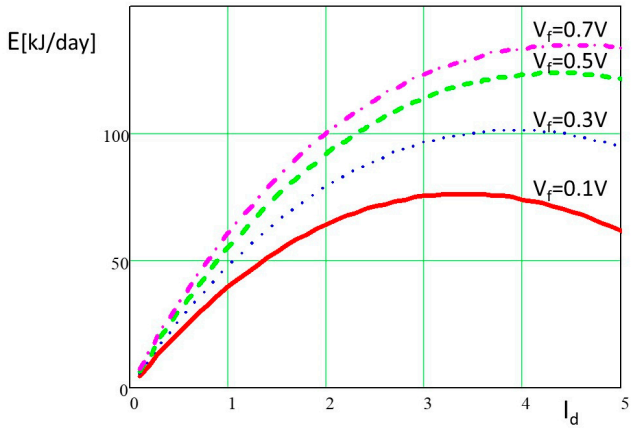

Figure 16. Energy production from the CapMix cell at constant current I_d [A].

Whatever the strategy chosen, all the previous figures show that, when evaluating the energy per day, it is not only the energy provided by the cell in each cycle that is important, but also the time it takes to extract it. The selection of $V_f \neq 0$ implies generating a short circuit in the cell to cause the rapid discharge of the remaining energy, in order to always start the water replacement process in the cell from the same conditions.

Also, it must be noted that these calculations have been ensured using a deionization cell that is designed for desalination, not for energy production. Energy production will increase if an optimized cell is used. Two parameters in particular must be improved: (a) the total series resistance should be reduced (by improving the material and components used [45]) in order to increase the discharge current and hence reduce the time involved in the energy extraction; and (b) the processed water volume must also be reduced to minimize the time involved in the pumping process and hence increase the daily number of cell charges and discharges.

Once the daily energy production has been estimated, the tests focus on determining how the converter used during the energy extraction penalizes the efficiency as a function of the current flowing through the inductor. This is done by varying the converter output voltage from 10 V to 200 V and, for each of these voltages, setting the hysteresis control to obtain a current ranging from 0.5 A to 10 A. By doing so, it is possible to determine the efficiency evolution of the converter as a function of the previous parameters, which helps us to study the efficiency of the power transfer from the CapMix cell to the grid. Using synchronous rectification instead of diodes D1 and D2 (see Figure 6) will also contribute to improving the efficiency of the power transfer.

Equations (16) and (17) can be used, respectively, to calculate the conduction losses, P_{cond}, and the switching losses, P_{sw}, during one cycle of the converter for a given value of the maximum current through the inductor, I_{Lmax}.

$$P_{cond} = (R_{ON} + R_L) \cdot \frac{I_{Lmax}^2}{3 \cdot \left(1 + \frac{V_{cell}}{V_o}\right)} + (R_{ON} + R_L) \cdot \frac{I_{Lmax}^2}{3 \cdot \left(1 + \frac{V_o}{V_{cell}}\right)} \tag{16}$$

$$P_{sw} = \left(E_{ON} \cdot \frac{I_{Lmax}}{80} + E_{OFF} \cdot \frac{I_{Lmax}}{80}\right) \cdot \frac{1}{I_{Lmax} \cdot L \cdot \left(\frac{1}{V_{cell}} + \frac{1}{V_o}\right)} \tag{17}$$

These losses are used to determine the efficiency of the converter, as indicated above. The parameters E_{ON}, E_{OFF} and R_{ON} used in these equations have been obtained from the SiC UF3SC065007K4S datasheets. Figure 17 shows the results obtained. It can be seen that increasing the inductor current makes the converter efficiency increase up to a maximum point, after which any subsequent increase in the inductor current brings about a reduction

in the converter efficiency, mainly because of the increase in conduction losses. Conduction losses have a linear relationship with the series resistance of both the inductor and the switches; minimizing the value of this resistance will result in improved converter efficiency. Figure 17 shows that switching losses also have an important effect on the efficiency; therefore, the inclusion of techniques involving soft switching significantly improves the overall performance. Note that the output voltage, Vo, has almost no influence in the system's efficiency. However, the value of the voltage across the equivalent capacitor of the CapMix cell, Vc, does have special relevance to the converter's efficiency. Figure 17 evinces that when this voltage increases, the output power increases correspondingly, but the losses produced will not vary significantly, thus resulting in improved performance.

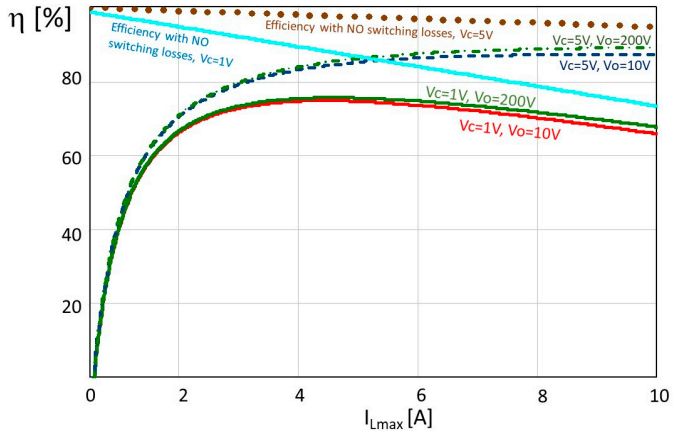

Figure 17. Evolution of the converter's efficiency as a function of current for various values of output voltage, Vo, and voltage across the internal equivalent capacitor, Vc.

It is also easy to understand that a reduction in the series resistance of the CapMix cell, R_S, will also have a clear influence on the efficiency, the same as the series resistance of the inductor and the switches. The importance of minimizing this value at the cell is more evident when the discharge current increases to generate more cycles per day.

Figure 18 shows the effect of the inductance value used in the converter. Reducing the inductance value will involve higher switching losses (frequency increases), and therefore, lower efficiency. This effect is attenuated as the value of the inductance increases due to the fact that the weight of the switching losses with respect to the conduction losses becomes smaller. On the other hand, there is no need to move to very large inductor values, since there is a point above which increasing the inductance value does not result in noticeable efficiency improvements.

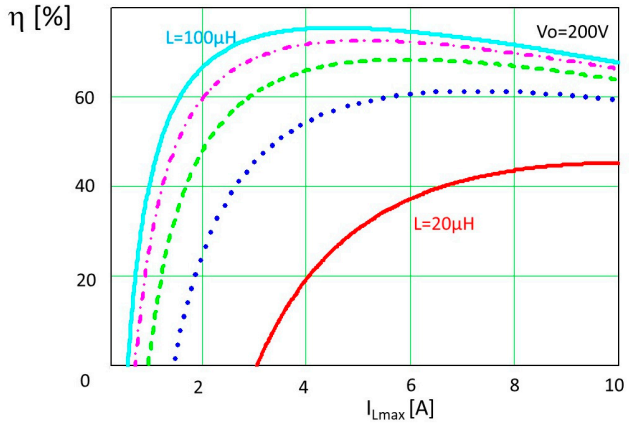

Figure 18. Variation of converter efficiency with several inductor values V_{Cell} = 1 V.

Using all the equations and plots presented here, it is possible to design the complete system and estimate the energy injected into the grid by directly multiplying the energy that can be extracted from the cell (discounting the losses that appear mainly in the series resistance) by the efficiency of the converter.

It might be thought that by reducing the discharge current, the conduction losses would be reduced and the efficiency of the converter would be improved, but the fact is that the duration of the discharge cycles would tend to take too long and the energy would be lost in parallel resistance (Figure 19). This figure also shows that, when considering the complete cell plus converter system, increasing the number of cells in series to raise the input voltage to the converter, V_{Cell}, results in an increase in the overall efficiency. This might suggest that the right strategy is connecting as many cells in series as possible. However, it must be taken into account that such an approach would give rise to a voltage imbalance between cells, not to mention the additional complexity associated with the construction of such cells: a voltage V_{Cell} = 1 V already requires a stack of 10 electrodes.

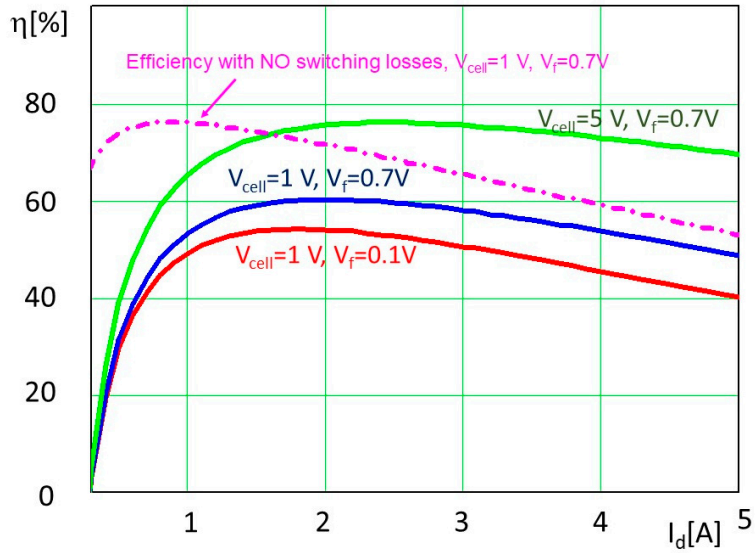

Figure 19. Variation of cell plus converter efficiency for several discharge currents.

5. Experimental Validation

To verify the correct operation of the bridgeless converter, some experimental results have been obtained: (a) with a battery and a supercapacitor as an element to store the energy; and (b) injecting the energy directly into the grid.

One important aspect to consider when designing the converter is the selection of the inductor that defines the switching frequency. In principle, lower values of L1 and L2 seem to be preferable, since they give rise to a higher operation frequency, making it possible to reduce the size of the output low-pass filter. However, Figure 18 shows that moving to very low values would penalize the efficiency. Taking this into account, the converters used for the tests include L1 = L2 = 80 μH, because this value is high enough to have almost negligible influence in the converter efficiency.

5.1. Energy Transfer to a Battery

Tests have been performed by replacing the load by up to three Li-ion modules in series (12.8 V, 7.5 A·h each). The currents through the inductor, I_L, and through the battery, I_{BAT}, are shown in Figure 20. In this case, a strategy of constant discharge current was selected, with the setpoint for the maximum inductor current being 2 A. Note that the inductor discharge process is very fast because of the high battery voltage used (38.4 V). To reduce the pulses in the charging current, a multiphase system is proposed (Figures 8 and 9) where several phase-shifted converters contribute with their output current to obtain low current ripple into the terminals of the battery.

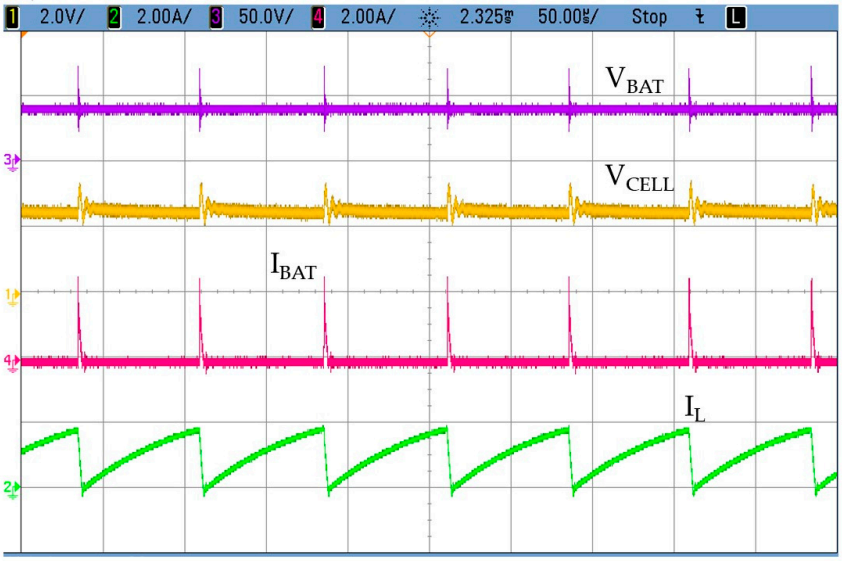

Figure 20. Power injection in a battery 38.4 V and 7.5 A·h.

To validate the theoretical analysis so far presented, the system's efficiency was determined using a different number of batteries in series as a load (Figure 21). The input voltage was fixed to 1.5 V, and two different inductors were used: L = 80 µH–20 mΩ and L = 50 µH–8 mΩ. As can be seen, the efficiency evolution depends not only on the inductance but also on the series resistance at the input path.

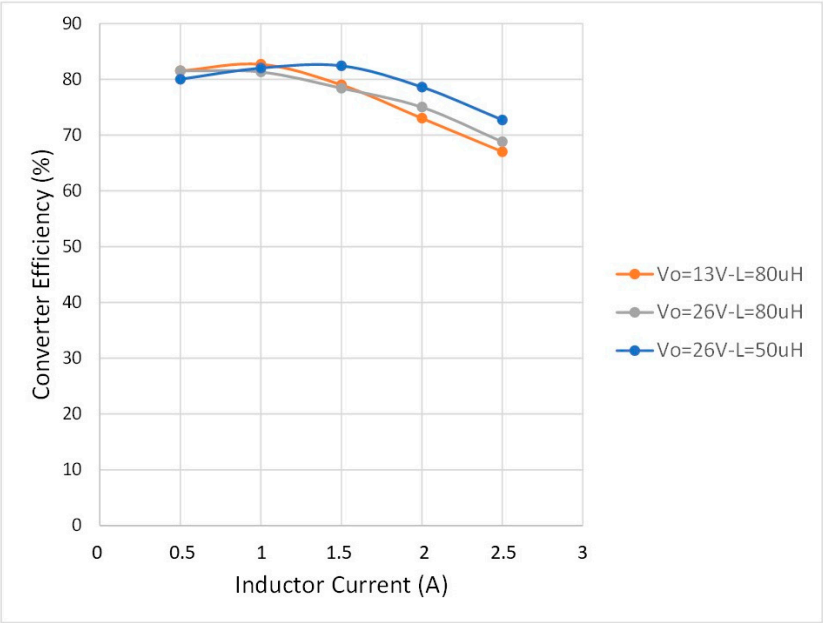

Figure 21. Measured evolution of the total system efficiency vs. inductor current for various output voltages and inductor values (input voltage: 1.5 V).

If a supercapacitor were used as an energy storage system (instead of a battery), it might be possible to have situations in which the voltage of this storage system was below that of the cell. In this case, the use of a buck–boost converter like the one in the testbench presented in this work will prove advantageous. Figure 22 shows that it is possible to inject energy into an initially uncharged supercapacitor (C = 22 F), giving rise to a linear charge evolution. In any case, the selection and optimization of the converter must be made for each individual situation. In the experimental test carried out, a 3 Apeak charging current was used. (Figure 22). The process takes 20 s to reach 2 V. The ultracapacitor rated

voltage is 2.7 V, and the maximum current rated is 15 A, which is 5 times higher than the one actually used. The manufacturer specifies 500,000 cycles as the projected cycle life at 25 °C, with a total capacity reduction of 30%, which guarantees the good stability and repeatablility of the test.

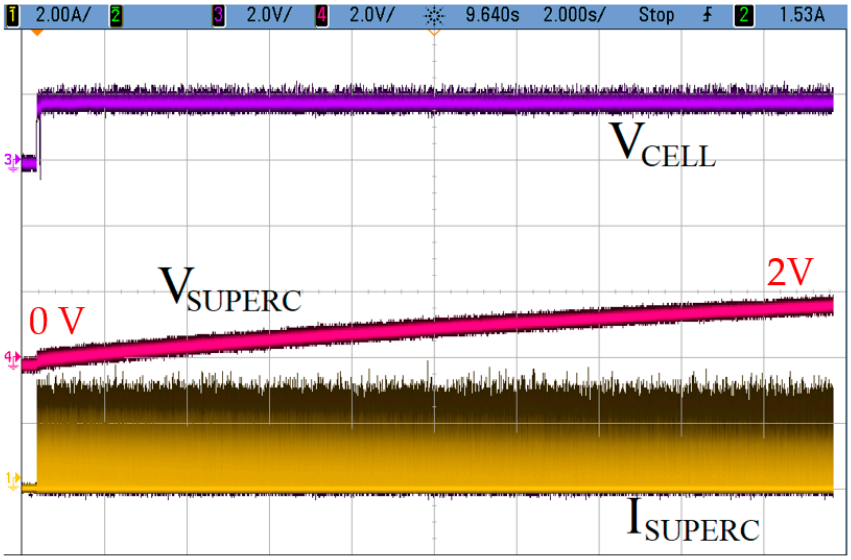

Figure 22. Power injection into an uncharged 22-F supercapacitor.

5.2. Energy Transfer to the Grid

Up to this point, the energy from the CapMix cell has been injected into a battery, and the setpoint for the maximum inductor current has always held a constant value. However, if the energy is to be transferred to the grid, this current reference can be proportional to the grid voltage, so as to make the current injected follow the sinusoidal evolution of the grid (Figure 23), thus contributing to power factor correction.

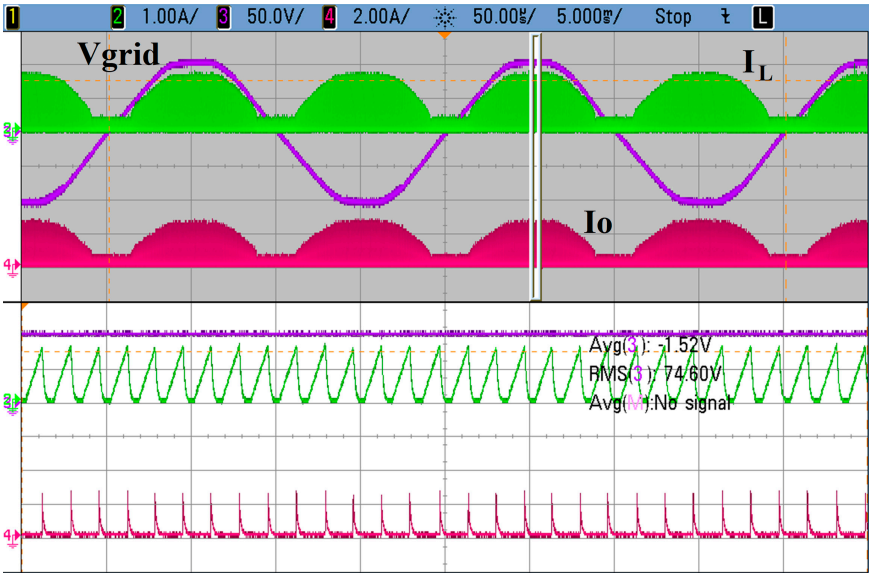

Figure 23. Current injection into the grid (V_{grid} = 150 V_{pk}). I_L: inductor current. I_O: bridgeless buck–boost output current.

We can observe from Figure 23 that the output current of the bridgeless buck–boost converter (I_O) also follows the sinusoidal shape of the AC grid voltage, although it is always positive. In order to have this current properly injected into the AC grid, it is necessary to add a non-autonomous inverter in the system so that current always flows into the positive

terminal (see Figure 10). The performance of the circuit when such an inverter is included can be seen in Figure 24. This figure also shows that, due to the high output voltage fixed by the grid, the inductor discharge is again very fast as compared with the time needed for the charging process.

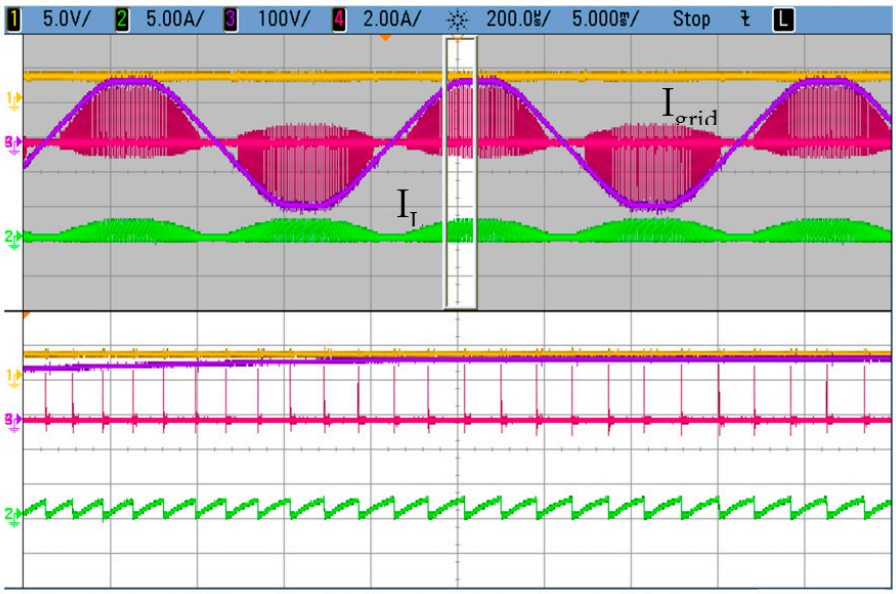

Figure 24. Current injection into the grid (V_{grid} = 200 V_{pk}). I_L: inductor current. I_{grid}: current injected into the grid.

Although the current thus injected into the grid is mainly formed by spikes, Section 3.4 has already indicated that it is possible to reduce high-frequency harmonics by connecting several bridgeless buck–boost converters in parallel to have a multistage interleaved converter that transfers the energy from the cells to the grid through the non-autonomous inverter [22–24].

6. Discussion

The generation of energy from different concentrations of salt in water is a technology currently being subhected to a very intense research process, where the study of new materials and their electrochemical behaviors plays a substantial role. Numerous studies have as a fundamental objective to obtain nanoporous carbons with a high effective surface area and high conductivity. On the other hand, the presence of ionic membranes also has a significant influence on the behavior of the cell. In general, the main scientific effort is oriented towards improving the electrochemical properties of the CapMix cell, but no attention has been paid to purely electrical aspects that can condition the extraction of the energy generated inside the cell.

In this article, we try to illustrate the problems associated with the injection of the energy generated in the CapMix cell into other energy storage elements (batteries, supercapacitors) or into the electrical grid itself. For this purpose, the behavior of the cell is analyzed by proposing an equivalent electrical model that allows us to incorporate it in electronic simulation programs together with the electronic converter in charge of injecting the energy from the cell into other systems. In this way, it is possible to identify the evolution of currents and voltages in order to determine the performance of the cell plus the power stage.

There are several aspects to take into account in order to optimize the efficiency and energy production of the cell plus converter system. On the one hand, we can minimize the series resistance of the cell, the inductor and the switches used in the converter, in order to reduce the discharge times of the cell (by using a larger discharge current) while maintaining acceptable conduction losses. Reducing the cell discharge time allows more

charge/discharge cycles to be performed during a day, thus increasing the energy production in this period (Equation (13)). The designs of the cell and the materials used are of particular importance, since they will determine the value of its series resistance, which will condition to a large extent the extraction of energy from the cell. Research on the development of ionic membranes and nanoporous carbons will improve the electrical performance of CapMix cells, hence increasing their energy production.

On the other hand, reducing the inductance value restricts the overall performance (Figure 18), since switching losses are increased. Soft switching techniques should be implemented in the converter to reduce the influence of this feature.

Another factor to take into account is the value of the voltage across the cell terminals (which plays the role of input voltage for the converter). Higher voltages at the input of the converter result in an increase in the converter efficiency, since more energy is processed for a similar value of losses. Unfortunately, cell complexity and issues associated with voltage equalization across the electrodes make it inadvisable to try to obtain cell voltages greater than a few volts.

The article presents a test bench to validate the possibility of injecting the energy generated in the CapMix cell into the two fundamental storage elements, the battery and supercapacitor, both with very different problems, and also directly into the electrical grid.

From the analysis carried out with the parameters measured in Voltea C-3 cells, it is concluded that the generation and transfer of energy from the CapMix cells to the grid and to other energy storage elements is viable. In the bibliography consulted, the energy generated by the cell is always applied on a resisitive load, where it is disspated. The work presented in this paper incorporates the electronics necessary to enable the use of this energy in the electricity system.

The daily energy production using ten C-3 cells is close to 140 kJ/day, which implies a specific energy of 1.3 Wh/kg. This value is low compared to Li batteries (150 Wh/kg), but falls within a range similar to that of supercapacitors (5 Wh/kg).

The efficiency of the CapMix cell when producing a voltage of 1 V reaches values in the order of 80% with the measured series resistance parameters. As far as the converter is concerned, using such a low input voltage will prevent high efficiency values. However, increasing the input voltage to 5–10 V would improve efficiency from 75% to 90% with the same components (close to 95% if soft switching is implemented). The problem is that constructing a CapMix cell that provides 10 V would require a stack of 100 electrodes in series and better manufacturing processes to avoid imbalanced voltages between electrodes.

Other than the equivalent parameters of the cell, what determines how much energy is generated daily is how fast we are able to transfer the energy from the cell to the grid. The less time it takes to extract the energy from the CapMix cell, the larger the number of charge/discharge cycles throughout the day (and hence the larger the total energy produced daily). In order to make this time as short as possible, it is important to use high discharge currents. The maximum value of the discharge current is limited by the series resistance of the cell, and will remain the same even if these cells are connected in series or parallel. Therefore, it is necessary to develop new materials that minimize series resistance, thus allowing higher currents and lower discharge times, which means more processed energy (charge/discharge cycles) per day.

Table 1 shows the most relevant features of some of the cells developed for technology assessment, and compares them with those present in the prototype developed for this work.

The demonstrator implemented allows for identifying different fields of study other than the optimization of the CapMix cell itself, such us the choice of the DC/DC converter that is best suited for a given application. But, even though some improvements can still be made, the results obtained show that it is feasible to use this technology with any storage element and obtain overall efficiencies that allow us to think of this type of renewable energy as an interesting option, bringing us closer to its commercialization.

Table 1. Comparison of the results presented and other CapMix cells in the literature.

Reference	Type	Volume (mm^3)	External Load (Ω)	Output Voltage (V)	Power Density (mW/m^2)
[6]	RED	___	5000		0.08
[7]	RED	$10 \times (43 \times 43 \times 0.5)$	___	1.48	$1 \div 1.5$
[12]	CDP	$100 \times 22 \times 15$	15	0.15	$20 \div 131$
[15]	CDP	$30 \times 60 \times 1.5$	1÷51	0.14	20.96
[16]	CDP	$8 \times (80\ cm^2 \times 0.15\ cm)$	Shortcircuit	0.148	200
[17]	CAPMIX	$10 \times 30 \times 0.4$	30	0.11	411
[18]	CDLE	$60 \times 60 \times 0.4$	11	0.098	32.6
[23]	CDLE	$30 \times 60 \times 0.5$	100	0.2	35
Paper presented	CAPMIX	Voltea C-3 Cell $240 \times 280 \times 280$	Grid, battery (38.4 V–7.5 A·h)	$38.4 \div 200$	Electrode surface unknown

7. Conclusions

This work presents the feasibility of using capacitive mixing cells (CapMix) to harvest energy from salinity gradient, and describes a method to obtain an electrical equivalent model that can be used to analyze the performance of this type of cell.

While several references can be found in the literature illustrating the capability of CapMix cells to harvest energy, there are not many works explaining how to efficiently extract this energy for a later use. This paper explores the possibility of injecting the energy available in a capacitive mixing cell into energy storage systems, such as a supercapacitor or battery, and also into the AC grid. A test bench is presented that uses current source injection to extract the energy and inject it into the storage system, which enables power factor correction at the grid level with simple circuitry. The actual electronic converter to be used must be analyzed in every individual case, but the general structure of the current-controlled converter used to extract the energy from the CapMix (followed by a synchronized inverter when necessary) has been proven adequate for this purpose.

Simulations have revealed that the maximum efficiency obtained when injecting energy into the AC grid was around 70%, and similar values were experimentally obtained. An increase in energy production would be achieved by reducing the series resistance of the cell and the volume of water processed.

The characteristics of the CapMix cell must still be improved before taking the commercialization step, but this paper demonstrates that this technology is already a real alternative for use in renewable energy production.

Author Contributions: This paper is part of the research carried out by A.M.P. and M.G.B., whereas J.A.M.-R. and J.A.M. assisted with the power stage and measurements. M.J.P. contributed with the design and modeling of the system. All authors have read and agreed to the published version of the manuscript.

Funding: This research was funded by the Predoctoral Program Severo Ochoa PCTI-FICYT under Grant PA-22-BP21-035, by the Research Challenges Program of the Spanish Ministry of Science under Grant MCI-20-PID2019-110971RB-I00, by the Government of the Principality of Asturias under Grant AYUD/2021/50938 and with the collaboration of HIDRITEC S.L.

Data Availability Statement: Data are contained within the article.

Conflicts of Interest: The authors declare no conflict of interest.

References

1. Qazi, A.; Hussain, F.; Rahim, N.A.; Hardaker, G.; Alghazzawi, D.; Shaban, K.; Haruna, K. Towards Sustainable Energy: A Systematic Review of Renewable Energy Sources, Technologies, and Public Opinions. *IEEE Access* **2019**, *7*, 63837–63851. [CrossRef]
2. IEA—International Energy Agency. Global Energy Review: CO2 Emissions in 2021. *IEA*. 2022. Available online: https://www.iea.org/data-and-statistics/data-product/global-energy-review-co2-emissions-in-2021 (accessed on 16 June 2022).

3. Jia, Z.; Wang, B.; Song, S.; Fan, Y. Blue energy: Current technologies for sustainable power generation from water salinity gradient. *Renew. Sustain. Energy Rev.* **2014**, *31*, 91–100. [CrossRef]
4. Simoncelli, M.; Ganfoud, N.; Sene, A.; Haefele, M.; Daffos, B.; Taberna, P.-L.; Salanne, M.; Simon, P.; Rotenberg, B. Blue Energy and Desalination with Nanoporous Carbon Electrodes: Capacitance from Molecular Simulations to Continuous Models. *Phys. Rev. X* **2018**, *8*, 021024. [CrossRef]
5. Yip, N.Y.; Brogioli, D.; Hamelers, H.V.M.; Nijmeijer, K. Salinity Gradients for Sustainable Energy: Primer, Progress, and Prospects. *Environ. Sci. Technol.* **2016**, *50*, 12072–12094. [CrossRef] [PubMed]
6. Hsu, W.-S.; Preet, A.; Lin, T.-Y.; Lin, T.-E. Miniaturized Salinity Gradient Energy Harvesting Devices. *Molecules* **2021**, *26*, 5469. [CrossRef] [PubMed]
7. Ju, J.; Choi, Y.; Lee, S.; Jeong, N. Comparison of fouling characteristics between reverse electrodialysis (RED) and pressure retarded osmosis (PRO). *Desalination* **2021**, *497*, 114648. [CrossRef]
8. Post, J.W.; Hamelers, H.V.M.; Buisman, C.J.N. Energy Recovery from Controlled Mixing Salt and Fresh Water with a Reverse Electrodialysis System. *Environ. Sci. Technol.* **2008**, *42*, 5785–5790. [CrossRef]
9. Pawlowski, S.; Crespo, J.; Velizarov, S. Sustainable Power Generation from Salinity Gradient Energy by Reverse Electrodialysis. In *Electrokinetics across Disciplines and Continents*; Ribeiro, A.B., Mateus, E.P., Couto, N., Eds.; Springer International Publishing: Cham, Switzerland, 2016; pp. 57–80. [CrossRef]
10. Sharma, M.; Das, P.P.; Chakraborty, A.; Purkait, M.K. Clean energy from salinity gradients using pressure retarded osmosis and reverse electrodialysis: A review. *Sustain. Energy Technol. Assess.* **2022**, *49*, 101687. [CrossRef]
11. Kim, J.; Lee, J.; Kim, J.H. Overview of pressure-retarded osmosis (PRO) process and hybrid application to sea water reverse osmosis process. *Desalin. Water Treat.* **2012**, *43*, 193–200. [CrossRef]
12. Sales, B.B.; Liu, F.; Schaetzle, O.; Buisman, C.J.; Hamelers, H.V. Electrochemical characterization of a supercapacitor flow cell for power production from salinity gradients. *Electrochim. Acta* **2012**, *86*, 298–304. [CrossRef]
13. Bijmans, M.; Burheim, O.; Bryjak, M.; Delgado, A.; Hack, P.; Mantegazza, F.; Tenisson, S.; Hamelers, H. CAPMIX -Deploying Capacitors for Salt Gradient Power Extraction. *Energy Procedia* **2012**, *20*, 108–115. [CrossRef]
14. Zhu, H.; Xu, W.; Tan, G.; Whiddon, E.; Wang, Y.; Arges, C.G.; Zhu, X. Carbonized peat moss electrodes for efficient salinity gradient energy recovery in a capacitive concentration flow cell. *Electrochim. Acta* **2019**, *294*, 240–248. [CrossRef]
15. Zou, Z.; Liu, L.; Meng, S.; Bian, X. Comparative study on the performance of capacitive mixing under different operational modes. *Energy Rep.* **2022**, *8*, 7325–7335. [CrossRef]
16. Liu, F.; Schaetzle, O.; Sales, B.B.; Saakes, M.; Buisman, C.J.N.; Hamelers, H.V.M. Effect of additional charging and current density on the performance of Capacitive energy extraction based on Donnan Potential. *Energy Environ. Sci.* **2012**, *5*, 8642–8650. [CrossRef]
17. Kim, T.; Rahimi, M.; Logan, B.E.; Gorski, C.A. Harvesting Energy from Salinity Differences Using Battery Electrodes in a Concentration Flow Cell. *Environ. Sci. Technol.* **2016**, *50*, 9791–9797. [CrossRef] [PubMed]
18. Sales, B.B.; Saakes, M.; Post, J.W.; Buisman, C.J.N.; Biesheuvel, P.M.; Hamelers, H.V.M. Direct Power Production from a Water Salinity Difference in a Membrane-Modified Supercapacitor Flow Cell. *Environ. Sci. Technol.* **2010**, *44*, 5661–5665. [CrossRef] [PubMed]
19. Burke, A. Ultracapacitors: Why, how, and where is the technology. *J. Power Sources* **2000**, *91*, 37–50. [CrossRef]
20. Nasir, M.; Nakanishi, Y.; Patmonoaji, A.; Suekane, T. Effects of porous electrode pore size and operating flow rate on the energy production of capacitive energy extraction. *Renew. Energy* **2020**, *155*, 278–285. [CrossRef]
21. Rica, R.A.; Ziano, R.; Salerno, D.; Mantegazza, F.; Van Roij, R.; Brogioli, D. Capacitive Mixing for Harvesting the Free Energy of Solutions at Different Concentrations. *Entropy* **2013**, *15*, 1388–1407. [CrossRef]
22. Brogioli, D.; Ziano, R.; Rica, R.; Salerno, D.; Kozynchenko, O.; Hamelersand, H.; Mantegazza, F. Exploiting the spontaneous potential of the electrodes used in the capacitive mixing technique for the extraction of energy from salinity difference. *Energy Environ. Sci.* **2012**, *5*, 9870–9880. [CrossRef]
23. Zou, Z.; Liu, L.; Meng, S.; Bian, X.; Li, Y. Applicability of Different Double-Layer Models for the Performance Assessment of the Capacitive Energy Extraction Based on Double Layer Expansion (CDLE) Technique. *Energies* **2021**, *14*, 5828. [CrossRef]
24. Seleym, A.; Elshafei, M. A new energy-efficient topology for solar-powered capacitive deionization systems. In Proceedings of the 2017 IEEE Electrical Power and Energy Conference (EPEC), Saskatoon, SK, Canada, 22–25 October 2017; pp. 1–6. [CrossRef]
25. Mehrabian-Nejad, H.; Farhangi, B.; Farhangi, S.; Vaez-Zadeh, S. DC-DC converter for energy loss compensation and maximum frequency limitation in capacitive deionization systems. In Proceedings of the 2016 7th Power Electronics and Drive Systems Technologies Conference (PEDSTC), Tehran, Iran, 16–18 February 2016; pp. 211–216. [CrossRef]
26. Baum, L.; Schumann, M.; Grumm, F.; Schulz, D. Large-signal time-domain equivalent circuit model for PEM fuel cell stacks. *Int. J. Hydrogen Energy* **2023**, *52*, 1285–1299. [CrossRef]
27. Alkuran, M.; Orabi, M. Utilization of a buck boost converter and the method of segmented capacitors in a CDI water purification system. In Proceedings of the 2008 12th International Middle-East Power System Conference, Aswan, Egypt, 12–15 March 2008; pp. 470–474. [CrossRef]
28. Pernía, A.; Alvarez-González, F.J.; Díaz, J.; Nuño, P.V.F. Optimum Peak Current Hysteresis Control for Energy Recovering Converter in CDI Desalination. *Energies* **2014**, *7*, 3823–3839. [CrossRef]
29. Jiya, I.N.; Gurusinghe, N.; Gouws, R. Electrical circuit modelling of double layer capacitors for power electronics and energy storage applications: A review. *Electronics* **2018**, *7*, 268. [CrossRef]

30. Laldin, O.; Moshirvaziri, M.; Trescases, O. Optimal power flow for hybrid ultracapacitor systems in light electric vehicles. In Proceedings of the 2011 IEEE Energy Conversion Congress and Exposition, Phoenix, AZ, USA, 17–22 September 2011; pp. 2916–2922. [CrossRef]
31. Pernia, A.M.; Alvarez-Gonzalez, F.J.; Prieto, M.A.J.; Villegas, P.J.; Nuno, F. New Control Strategy of an Up–Down Converter for Energy Recovery in a CDI Desalination System. *IEEE Trans. Power Electron.* **2014**, *29*, 3573–3581. [CrossRef]
32. Shanmugapriya, P.; Bengeri, P.M.; Dhanya, K.; Dakshina, R.; Abinaya, V. Hybridization of Supercapacitor and Battery for Fast Charging of Electric Vehicles. In Proceedings of the 2022 International Conference on Power, Energy, Control and Transmission Systems (ICPECTS), Chennai, India, 8–9 December 2022; pp. 1–5. [CrossRef]
33. Abadi, S.A.G.K.; Choi, J.; Bidram, A. A Method for Charging Electric Vehicles with Battery-Supercapacitor Hybrid Energy Storage Systems to Improve Voltage Quality and Battery Lifetime in Islanded Building-Level DC Microgrids. *IEEE Trans. Sustain. Energy* **2023**, *14*, 1895–1908. [CrossRef]
34. Han, X.-W.; Zhang, W.-B.; Ma, X.-J.; Zhou, X.; Zhang, Q.; Bao, X.; Guo, Y.-W.; Zhang, L.; Long, J. Review—Technologies and Materials for Water Salinity Gradient Energy Harvesting. *J. Electrochem. Soc.* **2021**, *168*, 090505. [CrossRef]
35. Huber, L.; Jang, Y.; Jovanovic, M.M. Performance Evaluation of Bridgeless PFC Boost Rectifiers. *IEEE Trans. Power Electron.* **2008**, *23*, 1381–1390. [CrossRef]
36. Bist, V.; Singh, B. An Adjustable-Speed PFC Bridgeless Buck–Boost Converter-Fed BLDC Motor Drive. *IEEE Trans. Ind. Electron.* **2014**, *61*, 2665–2677. [CrossRef]
37. Wang, Y.; Wang, Z.; Chen, B.; Wang, H. Analysis of Mathematical Modeling of Soft Switching in Synchronous Rectification Boost Converter. In Proceedings of the 2022 IEEE Applied Power Electronics Conference and Exposition (APEC), Houston, TX, USA, 20–24 March 2022; IEEE: Piscataway, NJ, USA, 2022; pp. 737–742. [CrossRef]
38. Lin, B.-R.; Lin, L.-A. Implementation of an Interleaved AC/DC Converter with a High Power Factor. *J. Power Electron.* **2012**, *12*, 377–386. [CrossRef]
39. Lin, X.; Wang, F. AC–DC bridgeless buck converter with high PFC performance by inherently reduced dead zones. *IET Power Electron.* **2018**, *11*, 1575–1581. [CrossRef]
40. Chandran, C.; Chandran, L.R. Two switch buck boost converter for power factor correction. In Proceedings of the 2015 International Conference on Technological Advancements in Power and Energy (TAP Energy), Kollam, India, 24–26 June 2015; IEEE: Piscataway, NJ, USA, 2015; pp. 454–459.
41. Samavatian, V.; Radan, A. A novel low-ripple interleaved buck-boost converter with high efficiency and low oscillations for fuel cell applications. *Int. J. Electr. Power Energy Syst.* **2014**, *63*, 446–454. [CrossRef]
42. Wen, H.; Su, B. Hybrid-mode interleaved boost converter design for fuel cell electric vehicles. *Energy Convers. Manag.* **2016**, *122*, 477–487. [CrossRef]
43. Garrigós, A.; Sobrino-Manzanares, F. Interleaved multi-phase and multi-switch boost converter for fuel cell applications. *Int. J. Hydrogen Energy* **2015**, *40*, 8419–8432. [CrossRef]
44. Nguyen-Van, T.; Tanaka, R.A.K. A digital hysteresis current control for half-bridge inverters with constrained switching frequency. *Energies* **2017**, *10*, 1610. [CrossRef]
45. Lee, D.; Roh, J.S.; Hwang, I.; Jung, Y.; Lee, H.; Ock, I.W.; Kim, S.; Sun, S.; Yang, S.; Park, H.B.; et al. Multilayered Graphene-Coated Metal Current Collectors with High Electrical Conductivity and Corrosion Resistivity for Flow-Electrode Capacitive Mixing. *ACS Sustain. Chem. Eng.* **2022**, *10*, 7625–7634. [CrossRef]